Ocean Engineering 343 (2026) 123255

Contents lists available at ScienceDirect

Ocean Engineering

journal homepage: www.elsevier.com/locate/oceaneng

Research paper

Numerical investigation on the survivability of a novel oscillating body with adjustable draft system

Chen Xi [a,b,c], Jian Tan [b], George Lavidas [b], Hongyi Jiang [a,c,e,*], Shengjie Rui [d], Yujie Jiang [a,c], Zhen Guo [c,e]

[a] Ocean College, Zhejiang University, Zhoushan, 316021, China
[b] Department of Offshore Engineering, Delft University of Technology, the Netherlands
[c] Hainan Institute, Zhejiang University, Sanya, 572025, China
[d] Civil and Environment Department, National University of Singapore (NUS), 9 Engineering Drive 1, 117576, Singapore
[e] Zhejiang Province Key Laboratory of Offshore Civil Engineering and Materials, Zhejiang University, Hangzhou, 310058, China

ARTICLE INFO

Keywords:
Wave energy converter
Oscillating body
Adjustable draft
Extreme wave
Survivability

ABSTRACT

A critical challenge to the practical deployment of wave energy converters (WECs) is their vulnerability to extreme wave loads. This study proposes a novel design for an oscillating body-WEC, called adjustable draft WEC (ADWEC), which aims to enhance resilience under extreme wave conditions while maintain extraction efficiency at normal sea states. The present numerical simulations focus on the interaction between regular extreme waves and ADWEC in both fixed and dynamic conditions. It is found that the excitation force is highly sensitive to wave nonlinearities, appearing as an asymmetric excitation force in the horizontal direction and a double-peak phenomenon in the vertical direction. Increasing the draft can significantly reduce vertical loads and heave motion, thereby enhancing survivability by mitigating impact forces and buoyancy fluctuations. A shallower draft allows for greater heave amplitude and higher energy conversion, particularly under short-period conditions. The present findings reveal that the draft of the ADWEC has significant effects on the wave loads, hydrodynamic performance and energy extraction, which provides guidance to the practical design of WECs for survivability.

1. Introduction

As estimated, about 22 billion tons of carbon dioxide are expected to be emitted by 2025 (International Energy Agency, 2021), and there is still no strong sign of holding back global climate change (Li et al., 2023). To mitigate this threat, various ocean energy technologies are currently under research and development, which are expected to play an increasingly important role in the energy transition (Rui et al., 2025; Sun et al., 2024; He et al., 2025). Ocean energy includes wave energy (Shi et al., 2023; Jahangir et al., 2024), tidal energy (Xu et al., 2025) and ocean thermal energy (Keiner et al., 2024). Among these, wave energy stands out as one of the renewable resources with the highest energy density, with a technical potential of about 5600 TWh/yr (Maheen et al., 2023). Despite variation in the design and principle of operation, WECs can be primarily classified into oscillating body/flap (Wang and Dong, 2022; Jin et al., 2024; Benites-Munoz et al., 2024), oscillating water column (Cheng et al., 2022a; Xie et al., 2024; Ko and Tsai, 2025), and overtopping device (De Barros et al., 2023), which can be adapted to different marine environments and application scenarios (energy supply for islands, buoys, and marine pastures, or coupled with offshore engineering structures). However, compared to offshore wind and solar energy with mature design specifications and extensive engineering experience, wave energy technology is still in the "research and development" or "early deployment" stage (Rodríguez Claudio et al., 2018). The commercialization of WECs currently faces two main bottlenecks: low power production efficiency and poor survivability under harsh oceanic environments (Ransley et al., 2017).

One of the major hurdles for WECs to be used on a large scale is the higher levelized cost of electricity (LCOE) (Zhou et al., 2023). In this sense, enhancing the power capture efficiency has become one of the key factors in boosting the techno-economic competitiveness of WECs. A recently proposed WEC concept, namely adjustable-draft oscillating body, has demonstrated its potential in the power improvement by varying its hydrodynamic characteristics to match different incident sea states. Wen et al. (2018) combined the wave spectrum with the power spectrum of buoy and further utilized the Taguchi design method to

* Corresponding author. Ocean College, Zhejiang University, Zhoushan, 316021, China.
E-mail address: hongyijiang88@gmail.com (H. Jiang).

https://doi.org/10.1016/j.oceaneng.2025.123255
Received 13 August 2025; Received in revised form 1 October 2025; Accepted 19 October 2025
Available online 23 October 2025

develop a truncated conical WEC, incorporating the response surface method to determine the optimal draft depth. Along the same approach, Al Shami et al. (2019) employed numerical methods to investigate the effect of seven parameters, including draft, on the resonant frequency and bandwidth of a two-body WEC. Wang and Ringwood (2021) proposed an optimization method for a three-body articulated oscillating body-WEC to achieve optimal performance in a specific sea area, suggesting that the downstream buoy should have a larger draft.

The adjustable draft system can also contribute to the design of power take-off (PTO) systems. For instance, Tan et al. (2023) proposed an adjustable draft mechanism for point absorber WECs, which showed the potential of reducing the PTO size and a 20 % increase in output power compared to a fixed-draft buoy. Subsequently, Tan et al. (2022) investigated the effect of adjusting the buoy draft of a spherical buoy on the excitation force and explored its impact on the design of the PTO system. As an extended application of a single device, Cheng et al. (2022b) studied three oscillating body-WECs arrayed in a straight line and revealed that a smaller draft is more beneficial for capturing energy in short waves.

The above investigations on the draft of WECs demonstrated the advantages in terms of improved capture bandwidth (Li et al., 2023). However, due to changes in the motion patterns and wetted surfaces, the reliability of WECs with the adjustable draft system can be significantly impacted, particularly with regard to the survivability under extreme loading conditions. Thus, on top of maximizing the conversion efficiency, WECs must consider survivability solutions for extreme conditions (Musiedlak et al., 2020). Transient shocks and structural overload caused by the highest sea states may lead to catastrophic damage, and design experience gained from traditional large-scale offshore engineering structures is not easily applicable to wave energy devices with stronger dynamic response (Lou et al., 2019). The presence of nonlinear phenomena such as wave breaking, wave impact, and overtopping introduces greater uncertainty for the adjustable draft WEC. Studying the behavior of devices in extreme sea conditions is key to ensuring their survivability (Stuhlmeier et al., 2018).

A deep understanding of the immense fluid loads experienced in challenging environments can consolidate the design iteration cycles. Zhu et al. (2023) experimentally investigated a point-absorber WEC that can move in surge, heave and pitch, under focused waves. They showed that as the peak frequency increases, the heave and surge responses decrease, while the mooring force remains relatively insensitive to frequency. Giannini et al. (2022) proposed a preliminary design method for offshore WECs, emphasizing structural stability under harsh sea states. A nearshore pendulum-type WEC was developed and numerically assessed under 100-year return period lateral and longitudinal loads. The results indicated that the novel structure is lighter in weight and exhibits superior performance under extreme lateral loading conditions. Giannini et al. (2024) conducted physical experiments on their novel WEC, and their experimental results showed that the extreme loads in survival mode were reduced by 65 % compared to operational mode. Kamarlouei et al. (2024) developed a torus-shaped WEC and determined the optimal design parameters using optimization codes. The results indicate that the incorporation of a moonpool structure enhances survivability compared to conventional oscillating body-WECs. Stansby and Moreno (2020) investigated the hydrodynamic response of an array of oscillating body-WEC with mooring systems using a time-domain linear diffraction–radiation model, highlighting that the interaction of excitation and radiation forces between larger buoys is critical to the response of the system. Guo et al. (2018) studied the excitation force modeling of a 1:50 scale cylindrical oscillating body-WEC in a wave tank, revealing strong correlations between experimental and numerical results under various wave conditions. Shahroozi et al. (2022, 2023) investigated mooring line tension and motion response of oscillating body WECs under 50-year return period extreme sea states in moderate water depths, using WEC-Sim software simulations and physical experiments, and found that constant PTO damping effectively reduced peak mooring loads. Tagliafierro et al. (2022) studied a tensioned-moored WEC system using a smoothed particle hydrodynamics (SPH) method, and found that adjusting the PTO damping according to the actual sea state could prolong the service life. Ropero-Giralda et al. (2020) also utilized SPH to study the effect of high sea states on the dynamic response and critical region loads of the WEC system. They demonstrated that fully submerging the WECs during high sea states is more effective in protecting the devices than fixed modes or enlarged structural dimensions, and that an optimal submergence depth exists.

In summary, for fixed-draft WECs, the survivability of the system has been a major focus in the literature and has been investigated through numerical and experimental methods across different sea states. However, for adjustable-draft WECs, previous studies have mainly focused on the enhancement in the energy conversion capability of the buoy with an optimized draft depth, but the possible adverse impact of the adjustable draft on the increase in hydrodynamic loads under extreme sea states (and on the survivability and structural integrity of the system) remains rarely explored. Additionally, when subjected to large wave-induced loads, the system may be influenced by nonlinear dynamic response, leading to changes in the dynamic response and structural load-bearing capacity of the device.

This paper aims to investigate the survivability of an oscillating body-WEC integrated with an adjustable draft system under extreme sea states using computational fluid dynamics (CFD) simulations, focusing particularly on the effects of draft variation on wave loads. For this purpose, the study first examines the wave excitation on this novel device under both regular and extreme wave heights, which reveals the contribution of the variable draft system in modulating the hydrodynamic loads. Finally, this study examines the improvement in the motion and energy capture performance from integrating the adjustable draft system with the oscillating body-WEC. Furthermore, to accurately capture the nonlinear phenomena, a fully nonlinear numerical wave tank (NWT) based on CFD was developed to analyze the influence of wave parameters and draft on the overall wave loads and dynamic response of the system. The structure of this paper is as follows: Section 2 presents the three-dimensional non-linear CFD model and the associated mathematical equations. In Section 3, numerical convergence of the model is verified, followed by a comparison with experimental results to validate the numerical model. In Section 4 the numerical results from the simulated model are presented and discussed. Finally, the conclusions are summarized in Section 5.

2. Methodology

2.1. Conceptual design of the ADWEC

A schematic of the adjustable draft WEC (ADWEC) is shown in Fig. 1. The device includes a spherical buoy of radius R, which is allowed to perform heave motion under the constraint of the PTO system. The PTO system consists of a hydraulic cylinder, a high-pressure gas accumulator, a low-pressure gas accumulator, and a hydraulic motor. The bottom of the buoy is connected to the hydraulic cylinder through a thin rod, and the oscillating motion of the buoy drives the hydraulic piston. The hydraulic oil is compressed by the reciprocating motion and stored in the accumulator then subsequently generating electrical power. To maintain proper flow direction, the rectifying valve system restricts liquid from leaving the high-pressure gas accumulator E and prevents backflow into the low-pressure gas accumulator D. The PTO system is simplified as a linear damping system neglecting friction loss. In this system, the draft of the WEC is controlled by adjusting the ballast water through a ballast pump inside the buoy.

The ADWEC proposed in this study has innovations in both structural design and functional implementation compared to conventional oscillating body-WECs. The conventional oscillating body-WECs typically employ a fixed draft design, resulting in essentially fixed hydrodynamic characteristics that limit adaptability to varying sea states. This is

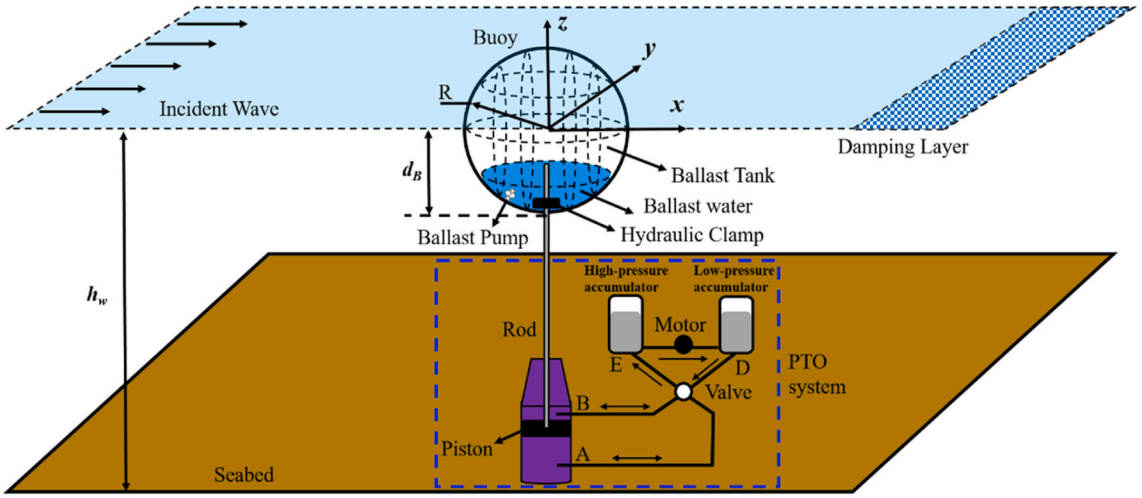

Fig. 1. Sketch of the three-dimensional adjustable draft WEC (ADWEC).

particularly critical under extreme sea states, where devices often face excessive responses and overwhelming loads. Adjusting the floater configuration can incur high operational and maintenance costs. The ADWEC enhances adaptability by incorporating an internal ballast tank and ballast pump to dynamically adjust the buoy draft in response to changing sea states. This approach facilitates an optimized balance between energy capture performance and structural survivability. More importantly, this adjustment not only changes mass distribution of the device, but also substantially affects its restoring force, waterplane area, and nonlinear hydrodynamic coupling characteristics, thereby modifying natural frequency and dynamic response behavior of the system. However, the influence of extreme loading conditions on the coupled dynamic require further clarification. The synergistic ability of structure and hydrodynamics enables ADWEC to have stronger adaptability and engineering practicality in complex environments. It overcomes the limitations of conventional devices in response control and environmental adaptability, offering significant value for practical deployment. In this setup, the buoy draft can be adjusted freely within its diameter range 2*R*. However, for buoys with relatively large draft, the buoy may completely submerge and then emerge during its motion, further leading to jumping out of the free surface. Under extreme sea conditions, this process could result in destructive consequences, such as structural damage, loss of energy conversion efficiency, or even complete system failure, for both the buoy and the PTO system. On the other hand, studies have shown that when the buoy draft is less than *R*, it is more likely to strike the water surface, leading to strong impact loads (Tan et al., 2023). Therefore, adjusting the buoy draft could help to avoid the aforementioned problems. In fact, reasonable minimum and maximum values of the draft are *R* and 1.5*R*, respectively (Tan et al., 2022).

To reduce the adverse impact of ballast water sloshing on the motion performance of the ADWEC, multiple ballast segments are installed inside the buoy. Each segment is either completely filled with water or completely emptied. Since the PTO is fixed to the seabed, the buoy draft will affect its stroke. Therefore, a hydraulic clamp is installed to adjust the length of the rod accordingly and the excess is stored in the buoy.

2.2. Numerical method

2.2.1. Governing equations for the flow

The interaction between extreme waves and ADWEC contains not only strong wave nonlinearity but also nonlinear fluid-structure interaction, such as large amplitude movements of the structure. Based on the incompressible viscous flow theory, a fully nonlinear 3D numerical model was developed using Star-CCM + software to accurately simulate the coupled process. The continuity equation and Navier-Stokes equations form the foundation for studying the hydrodynamic characteristics of the floating body. Due to incompressibility, the density of the fluid is constant. Mass conservation in the fluid domain is expressed by the continuity equation:

$$\frac{\partial u}{\partial x}+\frac{\partial v}{\partial y}+\frac{\partial w}{\partial z}=0 \tag{1}$$

where u, v, and w denote the velocity components in the x, y, and z directions, respectively.

The Navier-Stokes equations are expanded in the x, y, and z directions as follows:

$$\begin{aligned}
&\frac{\partial(\rho u)}{\partial t}+\nabla\cdot(\rho u\mathbf{v})=-\frac{\partial \rho}{\partial x}+\frac{\partial \tau_{xx}}{\partial x}+\frac{\partial \tau_{yx}}{\partial y}+\frac{\partial \tau_{zx}}{\partial z}+F_x\\
&\frac{\partial(\rho v)}{\partial t}+\nabla\cdot(\rho v\mathbf{v})=-\frac{\partial \rho}{\partial y}+\frac{\partial \tau_{xy}}{\partial x}+\frac{\partial \tau_{yy}}{\partial y}+\frac{\partial \tau_{zy}}{\partial z}+F_y\\
&\frac{\partial(\rho w)}{\partial t}+\nabla\cdot(\rho w\mathbf{v})=-\frac{\partial \rho}{\partial z}+\frac{\partial \tau_{xz}}{\partial x}+\frac{\partial \tau_{yz}}{\partial y}+\frac{\partial \tau_{zz}}{\partial z}+F_z
\end{aligned} \tag{2}$$

where ρ is the fluid density, F_x, F_y, and F_z represent the body forces in the x, y, z directions, respectively. For a Newtonian fluid, the viscous stress and the deformation rate of the fluid can be expressed as:

$$\begin{aligned}
&\tau_{xx}=2\mu\frac{\partial u}{\partial x}-\frac{2}{3}\nabla\cdot\mathbf{v}\\
&\tau_{yy}=2\mu\frac{\partial v}{\partial y}-\frac{2}{3}\nabla\cdot\mathbf{v}\\
&\tau_{zz}=2\mu\frac{\partial w}{\partial z}-\frac{2}{3}\nabla\cdot\mathbf{uv}\\
&\tau_{xy}=\tau_{yx}=\mu\left(\frac{\partial u}{\partial y}+\frac{\partial v}{\partial x}\right)\\
&\tau_{xz}=\tau_{zx}=\mu\left(\frac{\partial u}{\partial z}+\frac{\partial w}{\partial x}\right)\\
&\tau_{yz}=\tau_{zy}=\mu\left(\frac{\partial v}{\partial z}+\frac{\partial w}{\partial y}\right)
\end{aligned} \tag{3}$$

where μ is dynamic viscosity.

In the numerical solution, the Finite Volume Method (FVM) is used for spatial discretization of the Navier-Stokes equations since it is particularly suitable for solving flow problems with complex boundary conditions and irregular geometry. This method divides the computa-

tional domain into a large number of cells and directly integrates the mass, motion as well as energy conservation equations over each cell, ensuring that the physical quantities strictly satisfy the conservation laws. The Eqs. (1) and (2) can be represented by the general transport Eq (4).

$$\frac{d}{dt}\int_V \rho\phi dV + \int_A \rho\mathbf{v}\phi\cdot d\mathbf{a} = \int_A \Gamma\nabla\phi d\mathbf{a} + \int_V S_\phi dV \tag{4}$$

where ϕ represents an unknown variable (velocity component or pressure), A is the surface area of the cell, $d\mathbf{a}$ denotes the surface vector, Γ is diffusion coefficient and S_ϕ is source term. The terms, from left to right, are the transient term, the convective flux, the diffusive flux, and the source term. Fig. 2 illustrates the discretization of the transport equation on two polyhedral cells. The second-order midpoint method calculates the integral as the product of the unknown variable stored at the grid center and the cell face area.

$$\int_A \mathbf{J}^\phi \cdot d\mathbf{a} \approx \sum_f \mathbf{J}_f^\phi \cdot \mathbf{a}_f \tag{5}$$

where $\mathbf{J}^\phi$ is either the convective or the diffusive flux of fluid property ϕ, $\mathbf{a}_f$ is the surface area vector of face f of the cell, and $\sum_f$ is the sum over all cell faces of the cell.

2.2.2. Motion and energy conversion of the ADWEC

The floating body is treated as a rigid body undergoing only heave motion, and its equation of motion is expressed as:

$$(m + a_z)\ddot{\beta} + b_{pto}\dot{\beta} + c_{pto}\beta = f_g + f_w \tag{6}$$

where m is the mass of ADWEC, a_z is the linear added mass, $\ddot{\beta}$, $\dot{\beta}$ and β are the acceleration, velocity and displacement in the heave direction, respectively, b_{pto} and c_{pto} are damping and stiffness coefficients of the PTO system, respectively, f_g is the gravitational force on the ADWEC, and f_w is the wave force. The resonance frequency is defined as the natural frequency of the system when the inertial force and the restoring force are in equilibrium, which is calculated as:

$$\omega_n = \sqrt{\frac{c_{pto} + c_z}{m + a_z}} \tag{7}$$

The optimal PTO damping coefficient of a single body b_{opt} involving a single-mode motion with the wave frequency of ω can be obtained as (Cheng et al., 2023):

$$b_{opt} = \sqrt{\frac{\left((m + a_z)\omega^2 - (c_{pto} + c_z)\right)^2}{\omega^2} + {b_z}^2} \tag{8}$$

where b_z is the radiation damping coefficients of the floater. $c_z = \rho g A_w$ is the restoring force coefficient (A_w being the wetted surface of the ADWEC). The average wave energy conversion rate is given by:

$$E_p = \frac{1}{nT}\int_t^{t+nT} F\dot{\beta}dt = \frac{b_{pto}}{mT}\int_t^{t+nT} (\dot{\beta})^2 dt \tag{9}$$

where n is the number of wave periods, T is the wave period, t is the time, F is the combined external force on the ADWEC. The expression for the average energy flux rate E_w of linear waves is:

$$E_w = \frac{1}{8}\frac{\rho g H_I^2 \omega R}{k}\left(1 + \frac{2kh_w}{\sinh 2\,kh_w}\right) \tag{10}$$

where H_I is incident wave height, h_w is water depth, and k is wave number. The power generation performance of the ADWEC is measured by the conversion efficiency η, expressed as:

$$\eta = E_p / E_w \tag{11}$$

2.3. Computational domain and mesh

2.3.1. Numerical wave tank and boundary conditions

A 3D numerical wave tank was established to simulate the interaction between the ADWEC and 50-year return wave conditions from different sea areas, as shown in Fig. 3. The radius of the spherical ADWEC is R. The initial draft is the same as the radius while the origin of the Cartesian coordinate system is established at the geometric center of the device. In the NWT, the x-axis represents the direction of wave propagation, the y-axis the transverse direction, and the z-axis the vertical direction. The length of the NWT in the x direction is chosen as 8 times the wavelength (λ). The damping zone of 1.5λ is set at the rear end of the wave tank to eliminate the effects of wave-device interactions or wall reflections on the incident waves, providing a stable simulation environment. Furthermore, the z direction comprises both the gas and liquid phases. The height of the fluid domain is determined based on the water depth, while the gas phase is one-third of the water depth. Wave

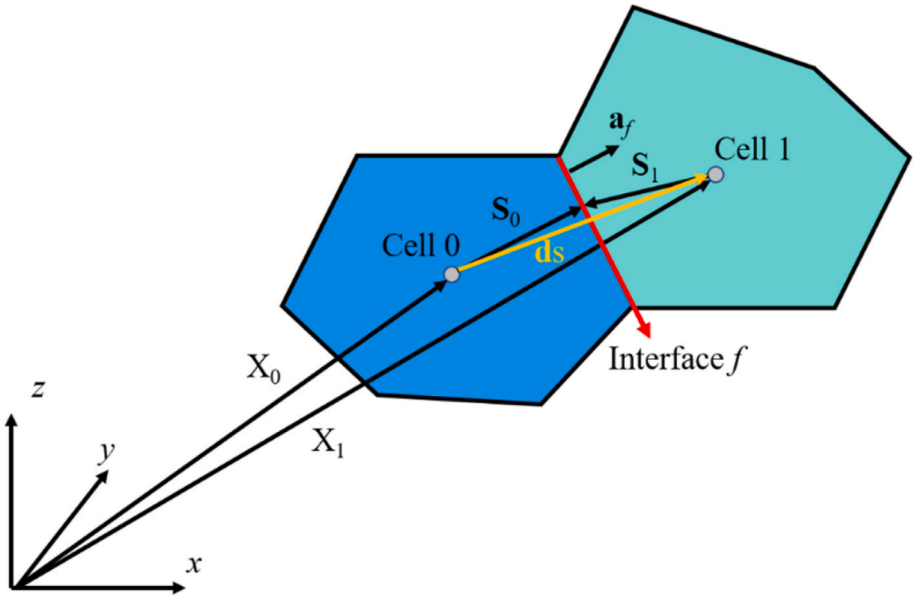

Fig. 2. Schematic for discretization of transport equations (Cheng et al., 2023).

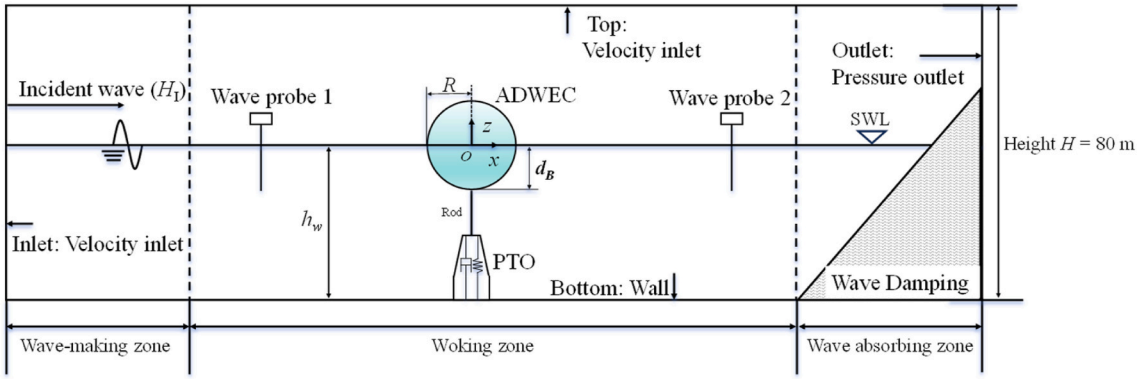

(a) Side view

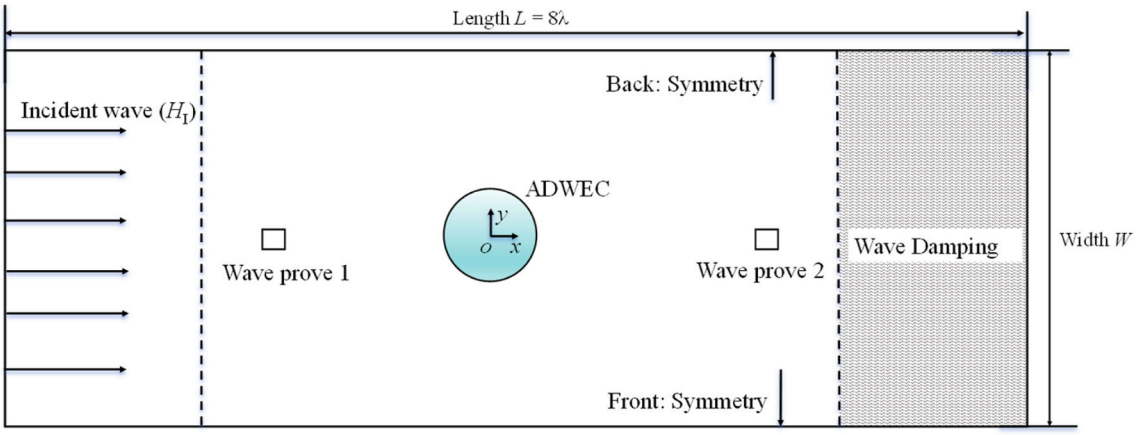

(b) Top view

Fig. 3. Sketch of the NWT and boundary condition settings for ADWEC in Star-CCM+.

probes are installed upstream and downstream of the device to check the incident waves and reflected waves at the end of the flume, respectively (Zhang et al., 2021). The Volume of Fluid (VOF) approach is used to track the free surface motion (Masoomi et al., 2023). Reynolds Averaged Navier-Stokes (RANS) equations are used to describe the turbulent motion of the fluid (Gao et al., 2023). A turbulence model, specifically the SST k-ω model, is introduced to close the RANS equations (Cheng et al., 2024).

Reasonable boundary conditions are critical to numerical simulations. The boundary locations and settings for the NWT are also given in Fig. 3. The left boundary condition is set as a velocity inlet, where fifth-order Stokes waves are applied to control the volume fraction and velocity of the multiphase (fluid and air phases) to generate extreme sea states. The right boundary is the pressure outlet, where the pressure is specified as the hydrostatic pressure of a fifth-order wave. The bottom boundary and the object surface are impermeable to water, so that these walls have no-slip condition. The front and back boundaries are symmetry planes.

2.3.2. *Mesh generation*

Both computational efficiency and modeling accuracy primarily rely on the mesh quality, in particular the mesh quality near the free surface and around the floating body. Fig. 4 shows the mesh for the present study. In particular, the free surface is divided by hexahedral cells based on the wave height, developing refinement and transition zones to ensure numerical stability. Since the overset mesh technique can flexibly handle large-amplitude motions, this approach is employed to apply finer mesh to the floating body. The overset mesh requires further definition of the background region and the overset zone adjacent to the ADWEC. These two zones can interact freely, by overlaying multiple small local cells on the background, allowing the overset mesh to capture details of the flow. Especially during object motion, the local cells can adapt to changes without the need to redevelop the entire mesh. It is worth noting that the complex flow characteristics under high sea states require the use of prism layer cells to meet the y^+ requirements of the turbulence model. Typically, 10–20 layers are applied along the surface of the body as a form of body-fitted mesh (shown in green). The complex air-water interface region is divided into simpler subdomains by discretizing mesh elements as described above. The flow in each subdomain is computed independently. The matching and coupling at the intersection of adjacent domains are performed using interpolation methods, which are dynamically identified based on the types of zones involved. Cells can be active, inactive, or dependent, corresponding to solved, ignored, and interpolated zones, respectively.

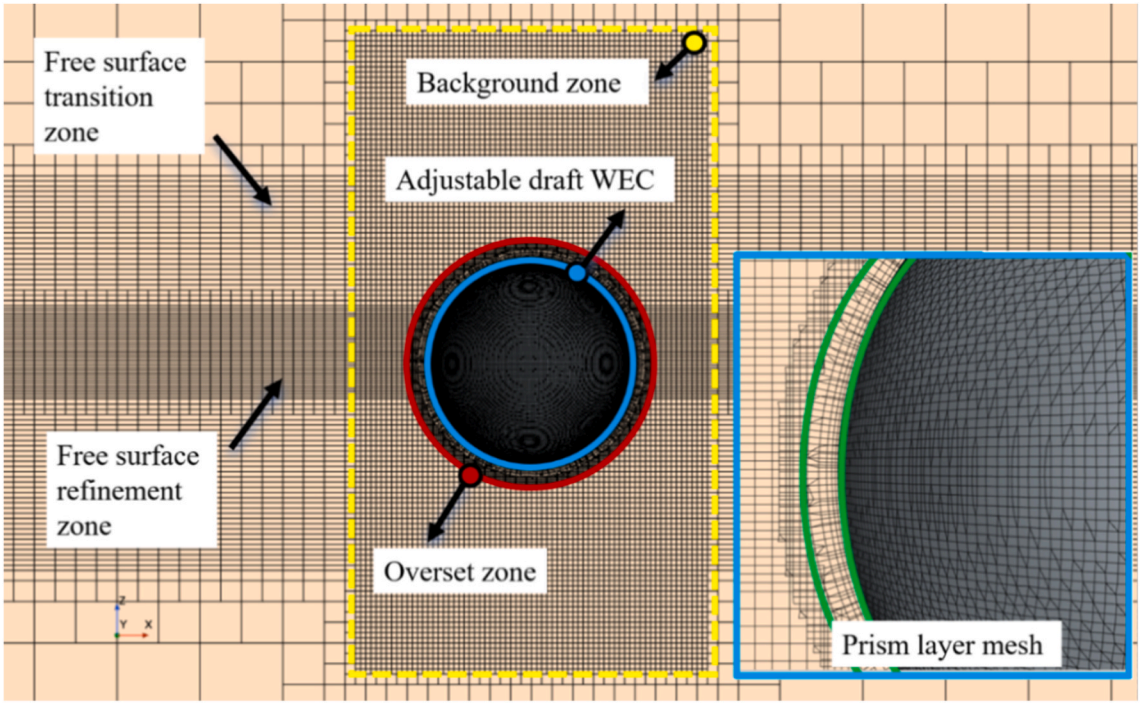

Fig. 4. Model mesh generation in side view.

3. Verification and Validation of the numerical results

3.1. Convergence test of the numerical wave tank

The width of the NWT in the *y*-direction affects wave propagation, body interactions, and the boundary effects of the fluid. In particular, the waves reaching the front and back boundaries may reflect, which may lead to inaccuracy in the numerical solution. To mitigate this effect, a convergence study is conducted on the width of the NWT. For the baseline model, the length L of NWT is 140 m, height H is 80 m, and the water depth h_w is 50 m. On this basis, four different widths are considered, with mesh blocks and corresponding mesh sizes specified in Table 1. Although a hydrostatic wave is used, mesh refinement and mesh transition along the water depth direction are still required. Hexahedral cells for these blocks are generated in the pre-processing step using the trimmed cell mesher. Differently, the overset mesh of buoy makes additional use of the surface remesher, which triangulates its surface to improve the overall quality. Prismatic layer mesher is used to accurately solve for the near-wall fluid. The heave free-decay of a 10 m diameter spherical WEC designed by Ocean Energy Systems (OES) Task 10 (Wendt et al., 2017) was simulated in the NWT. Its mass is 261799 kg, and at equilibrium position, the buoy had 5 m draft with its center of gravity located 2 m below the clam water surface. The initial displacement of the buoy is 0.1D and PTO damping is neglected. The blocks of the free surface cover the tank in both the x and y directions, where the height z of the refinement zone is 4 m, using $\triangle z_{re} = z_{re}/20$, $\triangle x_{re} = 4\triangle z_{re}$, $\triangle y_{re} = 6\triangle z_{re}$ (re denotess refinement zones) full scale to describe the mesh resolution. Two times the cell size of the refinement zone in each direction is used as the basis for meshing the transition zone. Based on the experimental study of the OES, the time step $\triangle t = T_{heave}/400$ was chosen, where T_{heave} is the period of the heave free-decay motion. Four models with different widths of NWT were studied, i.e., Case 1 (width = 80 m), Case 2 (width = 100 m), Case 3 (width = 120 m), Case 4 (width = 140 m).

Table 1
Mesh block and mesh size.

Block	x or R range (m)	y range (m)	z range (m)	Mesh size	Prism layer
Numerical wave tank	[-70, 70]	Case1: [-40, 40] Case2: [-50, 50] Case3: [-60, 60] Case4: [-70, 70]	[-50, 30]	Minimum absolute size = 0.5 m	/
Free surface refinement	[-70, 70]	[-10, 10]	[-2, 2]	$\triangle z_{re} = z_{re}/20$, $\triangle x_{re} = 4\triangle z_{re}$, $\triangle y_{re} = 6\triangle z_{re}$	/
Free surface transition	[-70, 70]	[-10, 10]	[-10, 8]	$\triangle z_{tr} = 2\triangle z_{re}$, $\triangle x_{tr} = 2\triangle x_{re}$, $\triangle y_{tr} = 2\triangle y_{re}$ (tr is transition zones)	/
Overset	6	/	/	$R_{overset}/60$	15

Fig. 5 shows the corresponding heave decay of the buoy for the four models. Case 1 with a width of 80 m is significantly different from the other three models after 15 s, showing an increasing trend in displacement. This difference can be attributed to rapid successive reflections of heave-induced radiation waves between the front and back walls. When the width is increased to 100 m in Case 2, the motion response at the same time is significantly reduced, though it still shows slight differences compared to the results of Case 3 and 4. The models with widths of 120 m and 140 m show good agreement in both phase and motion amplitude. The maximum relative error between Case 1 and Case 4 is 10.0 %, and the maximum relative error between Case 2 and Case 4 is 0.75 %. The results indicate that simulations with widths of 120 m and 140 m are appropriate. To achieve a balance between computational efficiency and the accuracy, the wave tank width from Case 3 was adopted in this study.

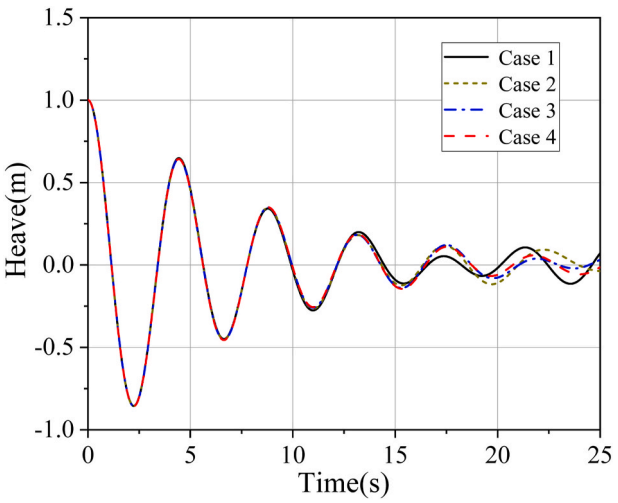

Fig. 5. Comparisons of heave decay for different NWT width.

3.2. Validation against experiment by OES Task 10

The OES Task 10 proposed by the International Energy Agency (IEA) aims to numerically model various WECs and evaluate the accuracy of numerical codes (Wendt et al., 2017). To analyze and validate the accuracy of the numerical model presented in this study, comparisons are made with the experimental results (Kramer et al., 2021). The geometry is regular, but taking the intersection between the sphere and the free surface into account both geometrical non-linearities as well as hydrodynamic non-linearities will be included. Firstly, the pre-defined NWT and mesh dimensions are implemented. Then, validations are performed for initial displacements of 1 m and 5 m, respectively, so as to prove the proficiency of the established NWT.

Fig. 6 presents the comparison of free decay results for different initial heights. As shown in Fig. 6(a), the present results are in good agreement with experimental results at an initial displacement of 0.1D (D denotes the diameter of the sphere). Additionally, the initial position 0.5D (the buoy is completely in the air) gives a large nonlinear disturbance of the free surface. At the same time, this comparison can further validate the ability of the present model to capture the strong nonlinearity of buoys in extreme sea states. The results of the present CFD model are compared with the experimental results from OES, showing a very good agreement in trend between the two results, as illustrated in Fig. 6 (b). Therefore, the present numerical framework is able to accurately model the strong nonlinear disturbances and the motion response of the floating body.

Subsequently, the present numerical model was compared with scaled experimental results by Andersen and Kramer (2023) to further validate the accuracy of the present model in simulating the interaction between regular waves and structures. The wave excitation forces were obtained by using a force sensor mounted on top of a fixed sphere with a diameter of 0.3 m. The submerged volume of a buoy is half its total volume. Test wave period is $T = 6.6$ s while wave height is $H_I = 0.6$ m. Fig. 7 displays the time series of the vertical wave excitation force on the buoy, non-dimensionalized by the initial buoyancy force F_{b0} of the sphere. As seen in Fig. 7, the good consistency demonstrates that the present model can accurately predict the wave excitation forces, exhibiting good agreement with experimental results.

4. Parametric study of the ADWEC

Based on the NWT dimensions and mesh details described in Sections 3, this section examines detailed interaction between extreme sea states and the ADWEC device. The focus is placed on assessing the effects of varying draft on wave excitation forces in the fixed mode, RAOs in the motion mode, and the corresponding impact on energy capture performance. The selection of extreme sea state refers to the shutdown conditions of the WaveStar device (Ghafari et al., 2021). Specifically, a wave height of 5 m was adopted as the input condition in this study

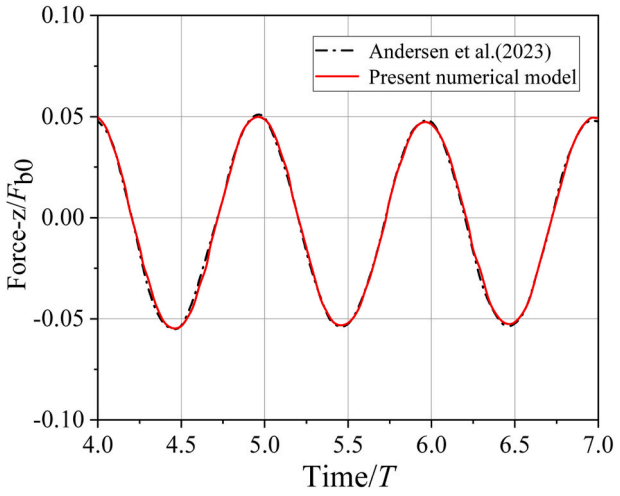

Fig. 7. Comparisons of the vertical excitation force between the present solutions and the experimental results.

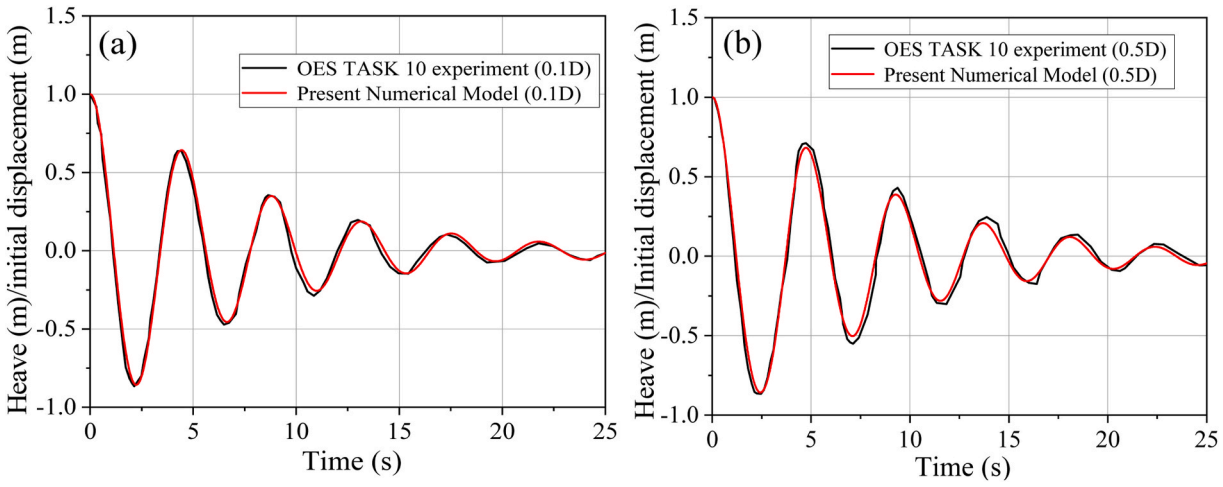

Fig. 6. Comparisons of heave decay between the present solutions and the experimental results.

(Karmer et al., 2011). All test sea states are based on regular waves, and the detailed sea states used in the tests are provided in Table 2. The ADWEC is designed based on OES TASK 10, with a spherical geometry of diameter $2R = 4$ m. In calm water, the initial draft is equal to the radius of floater, i.e., $d = 2$ m. Its mass is 16,755 kg. The center of gravity of the device is located 0.8 m below the free surface. In the initial state, the gravitational and buoyant forces are balanced, resulting in zero pretension in the PTO system. In practical applications, minimizing initial pretension is beneficial as it helps reduce mechanical wear and fatigue in PTO components.

4.1. Effect of wave nonlinearity

CFD is an essential tool for gaining in-depth understanding of the strong nonlinear effects induced by large wave heights under extreme sea states. First, the excitation force on a fixed buoy is simulated and presented in Fig. 8, where time series of forces in the x (Fx) and z (Fz) directions are displayed. Here, the results presented correspond to three regular wave tests with wave heights $H_I/R = 1.0$ and 2.5 and wave periods of $T = 8$ s, 10 s, and 12 s. With increasing wave height from 2 m to 5 m, both Fx and Fz exhibit significant amplification at the peaks. As shown in Fig. 8(a)–(c) and (e), waveforms of Fx become sharper across different periods, which is due to the Stokes waves stronger nonlinear structural features for $H_I/R = 2.5$.

Compared to $H_I/R = 1.0$, all three cases of $H_I/R = 2.5$ have a clear asymmetry in the excitation force of the wave propagation direction, i.e., the absolute values of the peaks are larger than those of the troughs. It indicates that Fx is most sensitive to waveform asymmetry induced by higher-order waves. This may be a nonlinear enhancement of the horizontal particle velocity at the wave crest. Additionally, during the transition between positive and negative wave excitation forces, a relatively steady time range with $Fx = 0$ is formed, followed by a sharp rise. This is because Fx primarily originates from the dynamic pressure, where the velocity is the key factor, and the velocity variation is very small in the transition zone from trough to wave front. Comparison of the maximum and minimum values of Fx shows that wave loading on the floater decreases with increasing wave period. Shorter wavelengths tend to generate more concentrated horizontal force.

Fig. 8(b)–(d) and (f) present the time series of vertical wave excitation forces acting on the ADWEC for different periods at $H_I/R = 1.0$ and 2.5. Compared with Fx, Fz has a better symmetry and is less affected by the incident wave asymmetry. Since the draft of ADWEC is equal to its radius, the geometric symmetry causes pressure variations near the free surface to cancel out in the vertical direction. With increase in the wave period, the peak value of Fz increases. The maximum Fz for periods 3.54, 5.32, and 7.09 at $H_I = 0.1$ are 1.29×10^5 N, 1.50×10^5 N and 1.57×10^5 N, respectively. Fz at large wave heights is significantly different from that at small wave heights. In a single wave period, Fz first reaches its maximum, followed by the appearance of local peaks as the wave propagates, while the minimum is not instantaneous and it remains stable for a certain period of time. The horizontal coverage of the incident wavelength is much larger than the diameter of the sphere, leading to a horizontally progressive enhancement of vertical excitation forces across different regions of the sphere, which forms two consecutive but staggered peaks. In other words, this phenomenon results from the combined effects of local wave-structure interaction and strong wave nonlinearity, which warrants particular attention under extreme conditions.

Table 2
Test sea states.

	Wave height (m)	Wave periods (s)				
General conditions	2m	8	10	12	14	16
Extreme sea state	5m					

4.2. Effect of the draft

Based on the findings in Section 4.1, neglecting nonlinear features such as peak values, local secondary peaks, and $Fz = 0$ during the interaction between extreme waves and the ADWEC may lead to a significant underestimation of structural impact risks. By adjusting the draft, the coupling effect between the structure and waves is altered, which directly affects the survivability. In order to investigate the influence of different drafts on the excitation force characteristics, three different drafts of $d_B = 1.0R$, $1.25R$ and $1.5R$ are considered, as shown in Fig. 9.

Fig. 10 displays the variation in the maximum Fz with draft under regular wave conditions representing severe sea states (wave height $H_I = 5.0$ m). Wave period is non-dimensional according to the acceleration due to gravity g and the water depth $h_w = 50$ m. The maximum Fz represents the peak value over the time series. As shown in Fig. 10, the maximum value of the vertical excitation force on the ADWEC increases with increasing wave period under the same draft. The primary reason is that the wavelength of the long-period wave is larger, and the extended time for the stronger wave pressure near the wave peak to act on the wet surface of the sphere. It is noteworthy that increasing the draft significantly reduces the peak of the wave excitation force. This indicates that increasing the submergence depth of the ADWEC can substantially improve the loading response. As wave-induced dynamic pressure is gradually reduced along the direction of increasing water depth, a deep-draft ADWEC significantly reduces the peak vertical excitation force by suppressing slamming effects and dynamic buoyancy fluctuations. Draft is further emphasized as a critical parameter in the excitation response and survivability of the regulatory device.

To quantify the response characteristics of vertical excitation with different drafts under strong regular waves, the peak and trough values of each time series of Fz were extracted, and the peak-to-trough ratio q was calculated as:

$$q = \left| \frac{Fz\text{-max}}{Fz\text{-min}} \right| \tag{12}$$

Fig. 11 displays the q value of the Fz as a function of wave period and draft. It can be concluded that for all wave period ranges, a greater draft has a positive effect on the slamming of the device. This is because the pressure of the wave peak is difficult to propagate to the deeper regions when the draft increases, avoiding periodic slamming, especially at $d_B = 1.5R$ with $q \ll 1$. Meanwhile, when the structure maintains a short draft ($d_B = 1.0R$), the q value approaches 1 as the wave period increases, indicating more symmetric dynamic loading. This is beneficial for stable operation and efficient PTO energy capture in practice.

4.3. Motion response

So far, the effect of the ADWEC in a fixed state has been studied. Nevertheless, this represents only a part of the overall boundary load analysis of the structure and does not encompass all cases. In practice, the device can absorb some wave energy through motion, thereby attenuating the concentrated loading of the excitation force. The amplitude of motion, capture efficiency and absorbed power for different drafts are examined based on the heave motion of the device. The optimal damping coefficient for different wave periods of the floater can be calculated using Eq. (8), with specific parameters shown in Table 3.

Fig. 12 displays the amplitude of motion, capture efficiency and absorbed power of the ADWEC as a function of the wave period and draft. As shown in Fig. 12(a), with increase in the draft, the motion response consistently decreases, with the motion at $d_B = 1.5R$ being the lowest among the three cases. The total mass of the floater is directly related to the displaced volume of water and a deeper draft results in greater inertia, thereby suppressing heave motion under the same

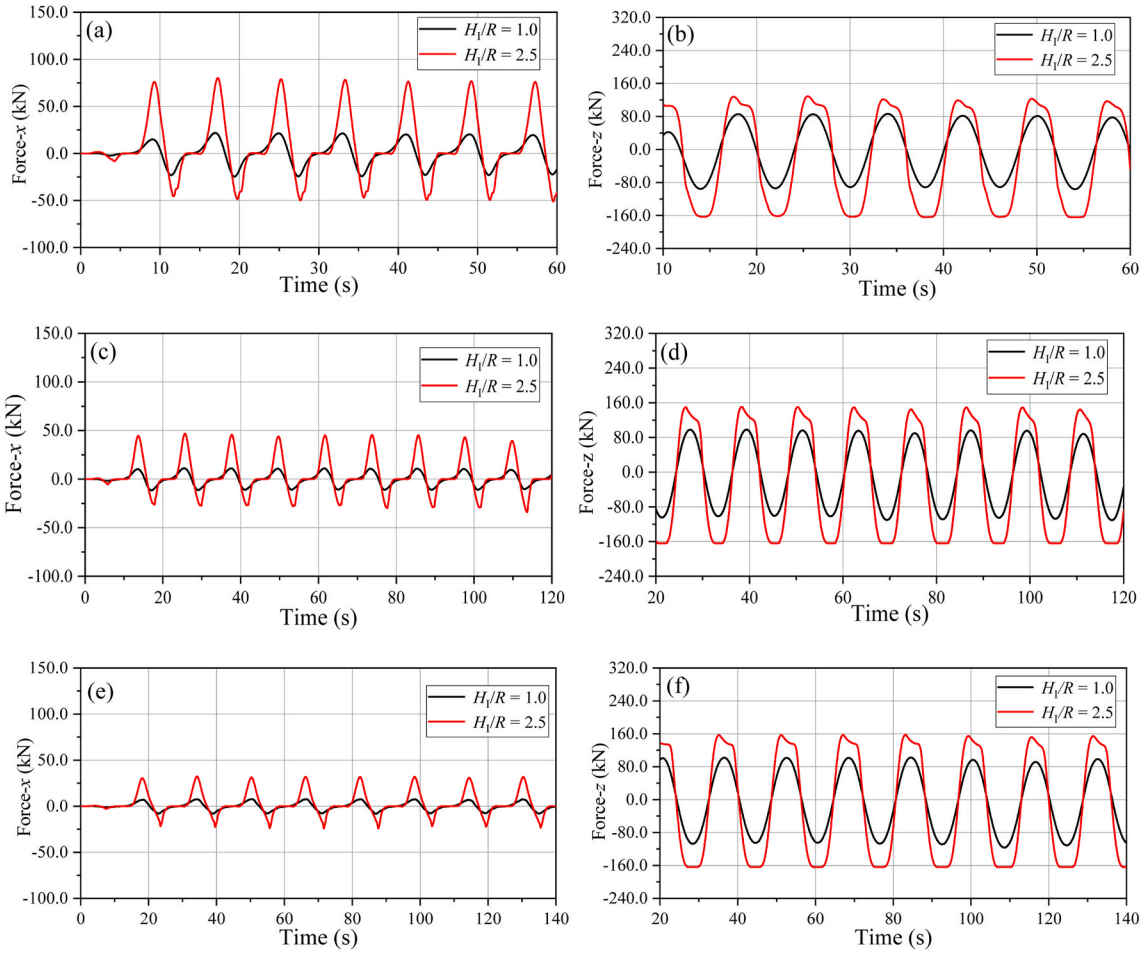

Fig. 8. Numerical estimated horizontal and vertical excitation forces on ADWEC (normal $H_I/R = 1.0$ and extreme $H_I/R = 2.5$ conditions) for three regular wave tests ($T = 8$ s (a and b), 10 s (c and d), and 12 s (e and f)).

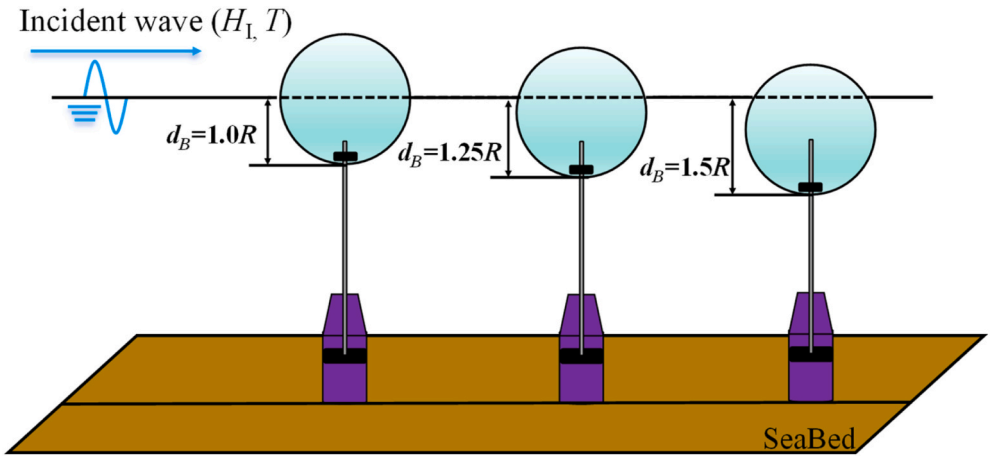

Fig. 9. Schematic of different drafts for ADWEC.

excitation force. Comparing the three drafts, it is seen that the motion amplitude decreases with increasing period at $d_B = 1.5R$ and then stabilizes, while the opposite is true for $d_B = 1.0R$ and $d_B = 1.25R$. This indicates that an excessively deep draft helps to improve the disturbance resistance and survivability of the device in long-period waves.

The variations in the absorbed power for all three drafts are similar, consistently decreasing with increasing period, as shown in Fig. 12(b). For the ADWEC, the case with $d_B = 1.0R$ yields the highest energy capture, reaching a maximum of 76089 W. This is because the frequency of long-period waves is far from the natural frequency of the device, making it difficult to match the maximum response range even with optimal damping. Compared to $d_B = 1.0R$, when the device draft is further submerged, the device capture energy is reduced because the wave dynamic energy is mainly concentrated at the free surface and decays exponentially with water depth. As plotted in Fig. 12(c), throughout the entire range of tested wave periods, the capture

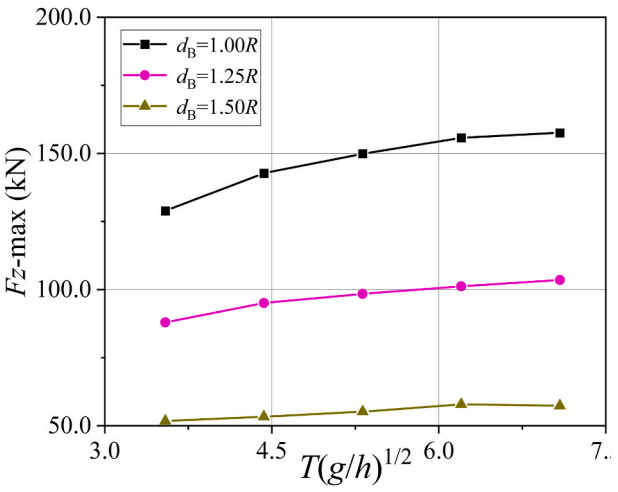

Fig. 10. Variations of the peak vertical wave excitation force *Fz*-max of ADWEC versus wave period $T(g/h)^{1/2}$ for different draft.

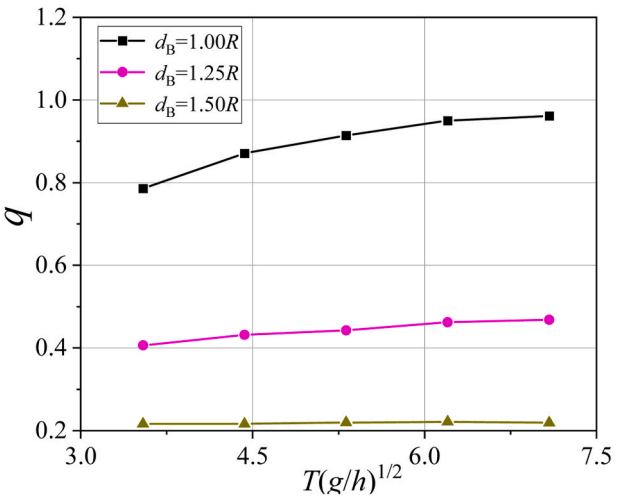

Fig. 11. Variations of the *q* factory of ADWEC versus wave period $T(g/h)^{1/2}$ for different drafts.

Table 3
The optimal PTO damping coefficient b_{opt}.

Wave periods	$d_B = 1.0R$	$d_B = 1.25R$	$d_B = 1.5R$
8s	132000	119000	86700
10s	176000	161000	122000
12s	218000	201000	156000
14s	218000	241000	188000
16s	301000	280000	220000

efficiency shows a significant decreasing trend with increasing period, reflecting the coupled effect of lower excitation frequency from long-period waves and reduced heave response.

In addition, the incident energy increases with longer wave periods, while the captured energy by the device actually decreases, ultimately decreasing the efficiency. Therefore, under normal conditions, maintaining a shallow draft enhances the heave response of the floater, which allows for improved energy conversion efficiency. It can be noted that the capture efficiency is highly dependent on the WEC draft. An increase of the WEC draft leads to lower capture efficiency. For instance, the capture efficiency of the WEC with a buoy draft of 1.0*R* is higher than that of 1.25*R* and 1.5*R* buoy drafts over a test range of wave periods. The largest draft corresponds to the lowest capture efficiency. A shallow draft enables the device to respond more rapidly to wave excitation, thereby enhancing the relative displacement and velocity between the buoy and the system. In contrast, a deeper draft increases the submerged volume, which reducing heave motion due to greater added mass, ultimately reduces energy transmission efficiency. In other words, although a deeper draft may reduce energy capture efficiency due to deviation from resonance, the associated reduction in hydrodynamic loads enhances the structural survivability of the device under extreme sea conditions. This demonstrates that draft not only changes the waterline area but also significantly influences the coupled dynamic response of the system. Whereas in extreme sea states, a deeper draft can be actively adopted to reduce structural loading at the expense of energy capture, thereby improving survivability.

5. Discussion

This paper proposes a novel WEC by integrating ballast tanks and ballast pumps into the oscillating body-WEC to enable draft adjustment. By adjusting its draft, the ADWEC can vary hydrodynamic characteristics, contributing to improved energy capture efficiency under regular sea states and reduced nonlinear load impacts under extreme conditions. However, the PTO system was simplified as an ideal model in this study. In practice, the actual PTO systems may be more complex due to their designs and types, which might lead to different nonlinear characteristics. For instance, in hydraulic PTO systems, the coupling of the hydraulic circuit with the other components makes the PTO force profile highly nonlinear. Therefore, further development of more realistic PTO systems is required to incorporate the effects of nonlinear forces into the research.

In this work, only regular waves are considered in the case study for a preliminary assessment. Given the real sea conditions when compared to other approaches, it is attractive to apply the CFD modelling to random and focused waves, which are characterized by strong nonlinearity between the waves and buoys. Thus, the next phase of this work is to introduce focused and random waves to each draft condition, and to evaluate the advantages of this configuration in terms of energy extraction or substitution benefits. Besides, the present numerical model has only been developed for an oscillating body-WEC with a single degree of freedom. However, as demonstrated by Ma et al. (2022), extending the modelling to multi-degree-of-freedom systems is feasible. Further verification is required to evaluate whether the present conclusions are directly applicable to a more practical 6-degrees of freedom scenario.

6. Conclusions

Excessive loading and strong nonlinearity of waves in extreme sea states seriously threaten the survivability of WECs. For commercial viability, a desirable design of the WEC is to allow for rapid adjustment of its hydrodynamic performance under dynamic sea states. In this study, a new oscillating body-WEC, i.e., the ADWEC, is proposed, whose main body is a spherical oscillating body with internal ballast tanks to control the draft, and the excess PTO link rods can be hidden inside the buoy.

An accurate CFD model of wave interaction with the ADWEC was established, and the model was then applied to investigate the hydrodynamic performance of the ADWEC numerically. The strong nonlinearity associated with large wave heights significantly affects the form of the wave excitation force acting on the buoy, while adjusting the draft can effectively reduce the loads. On this basis, the motion and energy capture performance of the buoy with different drafts were further investigated. The main conclusions can be drawn as follows.

(1) Unlike small wave heights, waves under extreme sea state (H_I = 0.1) produce a significant nonlinear excitation effect on the WEC

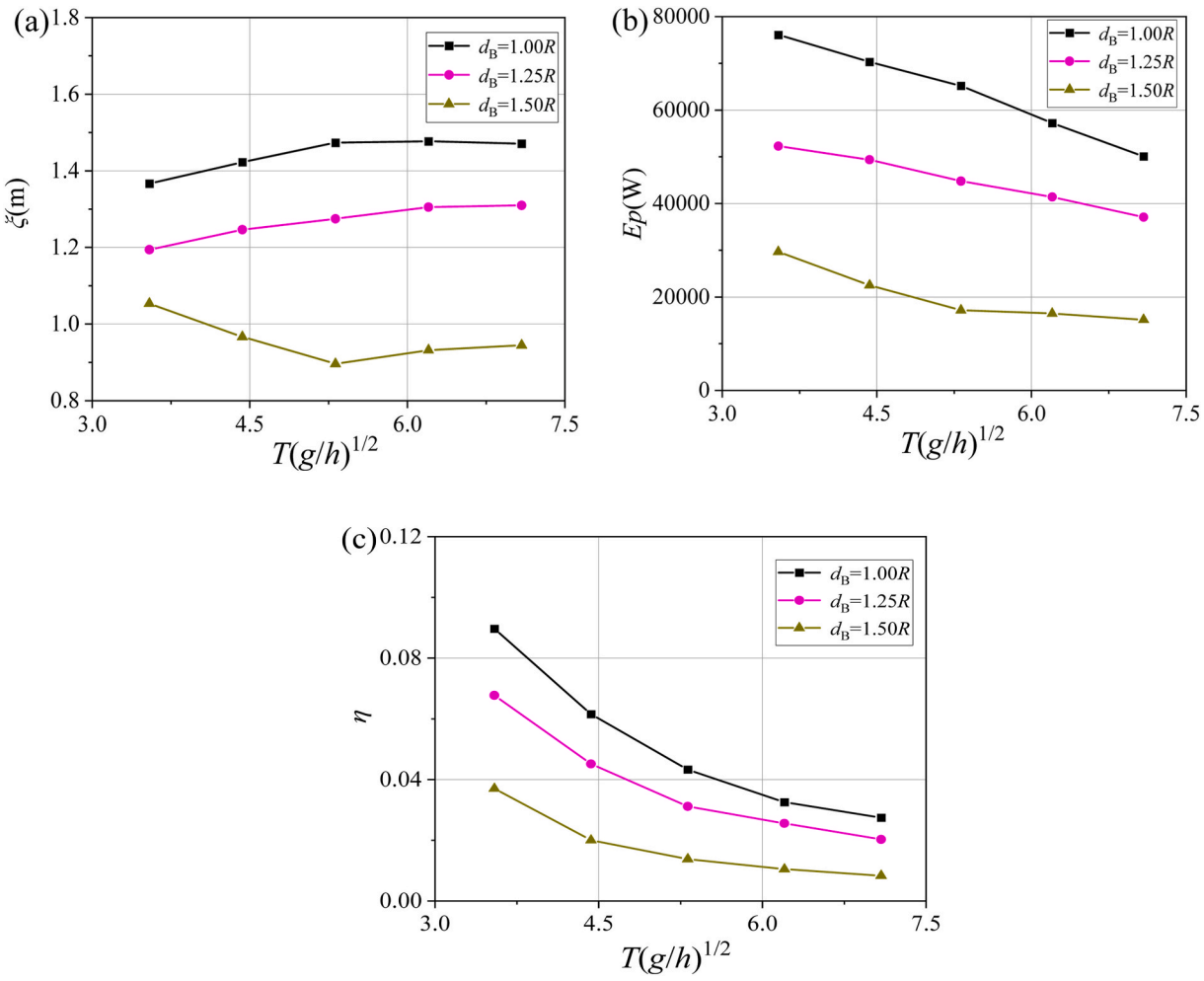

Fig. 12. Variations of (a) the amplitude of motion ξ; (b) the absorbed power E_p; and (c) the capture efficiency η versus wave period $T(g/h)^{1/2}$ for different ADWEC drafts.

at a fixed state. The horizontal excitation force *Fx* of the ADWEC exhibits strong asymmetry and amplification near the peak load. In comparison, although the vertical force *Fz* generally shows a more symmetric waveform, it also presents a continuous but time-staggered double-peak phenomenon during the wave peak phase. As the wave period increases, *Fx* is markedly reduced due to the decrease in horizontal thrust for long-period wave, while *Fz* shows relatively minor variation.

(2) The present numerical results indicate that adjusting the draft has a strong impact on the structural response and survivability. Similarly, in the fixed mode, the maximum vertical excitation force *Fz* decreases as the draft increases. This effectively mitigates wave impact and large fluctuations in dynamic buoyancy. Moreover, the defined q value also indicates that a deep-draft buoy ($d_B = 1.5R$) has a q-value less than 1, demonstrating a suppressing effect on impact loads.

(3) In the case of a constant wave height, as the draft increases, the displaced volume and mass also increase, enhancing its inertia. Consequently, heave motion is notably reduced, particularly at $d_B = 1.5R$ (the largest d_B considered in this study), where the response to long-period waves is further suppressed, displaying more powerful stability. Shallower drafts, on the other hand, can more effectively couple to the region of high energy near the free surface and achieve higher power absorption. In terms of energy conversion, the efficiency of all draft configurations decreases with increasing wave period. Overall, a shallow draft induces enhanced energy efficiency, while a deep draft contributes to improved survivability.

CRediT authorship contribution statement

Chen Xi: Writing – original draft, Validation, Supervision, Software, Methodology, Formal analysis, Data curation. **Jian Tan:** Writing – review & editing, Writing – original draft, Validation, Software, Formal analysis. **George Lavidas:** Writing – review & editing, Supervision, Investigation, Funding acquisition, Formal analysis, Data curation. **Hongyi Jiang:** Writing – review & editing, Supervision, Funding acquisition. **Shengjie Rui:** Writing – review & editing, Software. **Yujie Jiang:** Writing – review & editing, Investigation. **Zhen Guo:** Writing – review & editing, Investigation, Funding acquisition, Data curation.

Declaration of competing interest

The authors declare that they have no known competing financial interests or personal relationships that could have appeared to influence the work reported in this paper.

Acknowledgements

The authors would like to acknowledge the supports from the National Key R&D Program of China (2023YFB4203301, 2023YFB4203303), National Natural Science Foundation of China

(U24B20113, 52238008), the Zhejiang University Scholarship Program Funds supported Mr. Chen Xi's studies at the Delft University of Technology and Dutch Research Council (Nederlandse Organisatie voor Wetemschappelijk Onderzoek-NWO) (EP.1602.22.001).

Data availability

Data generated or analyzed during this study are provided in full within the published article.

References

Andersen, J., Kramer, M.B., 2023. Wave excitation tests on a fixed sphere: comparison of physical wave basin setups. In: Proceedings of the European Wave and Tidal Energy Conference, p. 15.

Al Shami, E., Wang, X., Zhang, R., Zuo, L., 2019. A parameter study and optimization of two body wave energy converters. Renew. Energy 131, 1–13.

Benites-Munoz, D., Huang, L., Thomas, G., 2024. Optimal array arrangement of oscillating wave surge converters: an analysis based on three devices. Renew. Energy 222, 119825.

Cheng, Y., Fu, L., Dai, S., Collu, M., Cui, L., Yuan, Z., Incecik, A., 2022a. Experimental and numerical analysis of a hybrid WEC-breakwater system combining an oscillating water column and an oscillating buoy. Renew. Sustain. Energy Rev. 169, 112909.

Cheng, Y., Song, F., Dai, S., Yuan, Z., Incecik, A., 2023. Broadband wave energy extraction by a dual-PTO hybrid system of a comb-type breakwater and an oscillating flap. Energy Convers. Manag. 297, 117670.

Cheng, Y., Song, F., Fu, L., Dai, S., Yuan, Z., Incecik, A., 2024. Experimental investigation of a dual-pontoon WEC-type breakwater with a hydraulic-pneumatic complementary power take-off system. Energy 286, 129427.

Cheng, Y., Xi, C., Dai, S., Ji, C., Collu, M., Li, M., et al., 2022b. Wave energy extraction and hydroelastic response reduction of modular floating breakwaters as array wave energy converters integrated into a very large floating structure. Appl. Energy 306, 117953.

De Barros, A., Fragassa, C., Paiva, M., Rocha, L., Machado, B., Isoldi, L., et al., 2023. Numerical study and geometrical investigation of an onshore overtop device wave energy converter with a seabed coupled structure. J. Mar. Sci. Eng. 11 (2), 412.

Gao, H., He, K., Guo, W., Gao, X., Li, B., Zou, J., Ding, S., Song, Y., 2023. Response power of floating three-body wave energy converter with different shapes. Sustain. Energy Techn. 57, 103225.

Ghafari, H.R., Ghassemi, H., He, G., 2021. Numerical study of the Wavestar wave energy converter with multi-point-absorber around DeepCwind semisubmersible floating platform. Ocean Eng. 232, 1–17.

Giannini, G., Rosa-Santos, P., Ramos, V., Taveira-Pinto, F., 2022. Wave energy converters design combining hydrodynamic performance and structural assessment. Energy 249, 123641.

Giannini, G., Zavvar, E., Ramos, V., Calheiros-Cabral, T., Iglesias, I., et al., 2024. On the development of a near-shore pivoting wave energy converter. Energies 17 (11), 2695.

Guo, B., Patton, R.J., Jin, S., Lan, J., 2018. Numerical and experimental studies of excitation force approximation for wave energy conversion. Renew. Energy 125, 877–889.

International Energy Agency (IEA), 2021. Net Zero by 2050 (A roadmap for the global energy sector). Available at: https://www.iea.org/reports/net-zero-by-2050.

Jahangir, M., Houmani, A., Kargarzadeh, A., 2024. A theoretical assessment of energy efficiency of wave tower as an oscillating wave surge converter. Ocean Eng. 295, 116748.

Jin, H., Zhang, H., Zheng, S., Xu, D., 2024. Characteristics of a two-dimensional periodic wave energy converter array. Renew. Energy 222, 119834.

Keiner, D., Langer, J., Gulagi, A., Satymov, R., Breyer, C., 2024. Future role of ocean thermal energy converters in a 100% renewable energy system on the case of the Maldives. Energy 312, 133620.

Ko, C., Tsai, C., 2025. Hydrodynamic performance of an OWC wave energy converter combined with a perforated wall. Ocean Eng. 327, 120955.

Kamarlouei, M., Hallak, T.S., Gaspar, J.F., Gaspar, F.J., Calvário, M., Soares, G.C., 2024. Torus-shaped wave energy converter attached to a hinged arm. J. Offshore Mech. Arctic Eng. 146 (1), 012003.

Kramer, M.B., Andersen, J., Thomas, S., et al., 2021. Highly accurate experimental heave decay tests with a floating sphere: a public benchmark dataset for model validation of fluid–structure interaction. Energies 14 (2), 269.

Kramer, M.L., 2011. Performance evaluation of the wavestar prototype. In: Proceedings of the 9th European Wave and Tidal Conference, pp. 5–9.

Li, Y., Li, Y., Guo, Z., Xu, Q., 2023. Durability of MICP-reinforced calcareous sand in marine environments: Laboratory and field experimental study. Biogeotechnics 1 (2), 100018.

Li, D., Sharma, S., Borthwick, A.G., Huang, H., Dong, X., Li, Y., Shi, H., 2023. Experimental study of a floating two-body wave energy converter. Renew. Energy 218, 119351.

Lou, J., Yim, S.C., Baker, J., Amon, E., von Jouanne, A., 2019. Field test study and quasi-static analysis of global characteristics and survivability of a wave energy converter test platform mooring system. J. Ocean Eng. Mar. Energy. 5, 283–300.

Ma, Y., Xie, G., Liu, S., Zhao, T., Zhu, Y., Zhang, X., 2022. Hydrodynamic performance investigation of the multi-degree of freedom oscillating-buoy wave energy converter. Ocean Eng. 285 (1), 115345.

Maheen, M.H., Yang, Y., 2023. Wave energy converters with rigid hull encapsulation: a review. Sustain. Energy Techn. 57, 103273.

Masoomi, M., Sarlak, H., Rezanejad, K., 2023. Hydrodynamic performance analysis of a new hybrid wave energy converter system using OpenFOAM. Energy 269, 126807.

Musiedlak, P.H., Ransley, E.J., Hann, M., Child, B., Greaves, D.M., 2020. Time-splitting coupling of wavedyn with openfoam by fidelity limit identified from a WEC in extreme waves. Energies 13 (13), 3431.

Ransley, E.J., Greaves, D., Raby, A., Simmonds, D., 2017. Hannet M. Survivability of wave energy converters using CFD. Renew. Energy 109, 235–247.

Rodríguez Claudio, A., Paulo, Rosa-Santos, Francisco, Taveira-Pinto, 2018. Assessment of the power conversion of wave energy converters based on experimental tests. Energy Convers. Manag. 173, 692–703.

Ropero-Giralda, P., Crespo, A.J., Tagliafierro, B., Altomare, C., Domínguez, J.M., et al., 2020. Efficiency and survivability analysis of a point-absorber wave energy converter using DualSPHysics. Renew. Energy 162, 1763–1776.

Rui, S., Jostad, H., Zhou, Z., Bachynski-Polić, E., Sævik, S., et al., 2025. Analysis of mooring system for floating wind turbine based on macro-model of chain-seabed interaction. Marine Structures 104, 103877.

Shahroozi, Z., Göteman, M., Engström, J., 2022. Experimental investigation of a point-absorber wave energy converter response in different wave-type representations of extreme sea states. Ocean Eng. 248, 110693.

Shahroozi, Z., Göteman, M., Engström, J., 2023. Control of a point absorber wave energy converter in extreme wave conditions using a deep learning model in WEC-Sim. OCEANS 2023-limerick IEEE 1, 10.

Shi, X., Li, S., Liang, B., Zhao, J., Liu, Y., Wang, Z., 2023. Numerical study on the impact of wave-current interaction on wave energy resource assessments in Zhoushan sea area, China. Renew. Energy 215, 119017.

Stansby, P.K., Moreno, E.C., 2020. Hydrodynamics of the multi-float wave energy converter M4 with slack moorings: time domain linear diffraction-radiation modelling with mean force and experimental comparison. Appl. Ocean Res. 97, 102070.

Stuhlmeier, R., Xu, D., 2018. WEC design based on refined mean annual energy production for the Israeli Mediterranean coast. J. Waterw. Port, Coast. Ocean Eng. 144 (4), 06018002.

Sun, X., He, J., Cui, H., Shi, J., 2024. Endeavours to achieve sustainable marine infrastructures: A new "window" for the application of biomineralization in marine engineering. Biogeotechnics 2 (4).

Tagliafierro, B., Martínez-Estévez, I., Domínguez, J., Crespo, A., Göteman, M., et al., 2022. A numerical study of a taut-moored point-absorber wave energy converter with a linear power take-off system under extreme wave conditions. Appl. Energy 311, 118629.

Tan, J., Polinder, H., Laguna, A., Miedema, S., 2022. A numerical study on the performance of the point absorber Wave Energy Converter integrated with an adjustable draft system. Ocean Eng. 254, 111347.

Tan, J., Polinder, H., Laguna, A., Miedema, S., 2023. A wave-to-wire analysis of the adjustable draft point absorber wave energy converter coupled with a linear permanent-magnet generator. Ocean Eng. 276, 114195.

Wang, L., Ringwood, J., 2021. Control-informed ballast and geometric optimisation of a three-body hinge-barge wave energy converter using two-layer optimisation. Renew. Energy 171, 1159–1170.

Wang, Y., Dong, S., 2022. Array of concentric perforated cylindrical systems with torus oscillating bodies integrated on inner cylinders. Appl. Energy 327, 120087.

Wen, Y., Wang, W., Liu, H., Mao, L., Mi, H., Wang, W., Zhang, G., 2018. A shape optimization method of a specified point absorber wave energy converter for the South China Sea. Energies 11 (10), 2645.

Wendt, F., Yu, Y., Nielsen, K., Ruehl, K., Bunnik, T., Touzon, I., et al., 2017. International Energy Agency Ocean Energy Systems Task 10 Wave Energy Converter Modeling Verification and Validation (No. NREL/CP-5000-68465). National Renewable Energy Lab (NREL).

Xie, G., Hu, C., Li, D., Ma, Y., Zhang, X., Zhu, Y., 2024. Hydrodynamic performance investigations of OWC and hybrid system: geometry of OWC and rectangular submerged breakwater. J. Mar. Sci. Eng. 12 (12), 2191.

Xu, S., Yu, F., Zhang, X., Wei, D., Diao, Y., Li, G., et al., 2025. Investigation of temporal and spatial distribution of tidal energy in Liuheng waterway via coastal acoustic tomography. Renew. Energy 240, 122180.

Zhang, H., Zhou, B., Zang, J., Vogel, C., Fan, T., Chen, C., 2021. Effects of narrow gap wave resonance on a dual-floater WEC-breakwater hybrid system. Ocean Eng. 225, 108762.

Zhou, B., Zheng, Z., Hong, M., Jin, P., Wang, L., Chen, F., 2023. Dynamic and power generation features of A wind–wave hybrid system consisting of A spar-type wind turbine and an annular wave energy converter in irregular waves. China Ocean Eng. 37 (6), 923–933.

Zhu, G., Shahroozi, Z., Zheng, S., Göteman, M., Engström, J., Greaves, D., 2023. Experimental study of interactions between focused waves and a point absorber wave energy converter. Ocean Eng. 287, 115815.

He, B., Yue, P., Zhu, Y., Liu, H., Guo, Z., Li, Y., 2025. Experimental study on hole erosion behaviors of marine soil solidified by an innovative organic composite material. Appl. Ocean Research 163, 104755.